Published in final edited form as:
Nucl Med Biol. 2008 January ; 35(1): 111–121.

Coligand Effects on Solution Stability, Biodistribution and Metabolism of ^{99m}Tc-Labeled Cyclic RGDfK Tetramer

Shuang Liu*, **Young-Seung Kim**, **Wen-Yuan Hsieh**, and **Subramanya Gupta Sreerama**

Abstract

In this study, we present the evaluation of two new ternary ligand ^{99m}Tc complexes [^{99m}Tc(HYNIC-tetramer)(tricine)(L)] (L = ISONIC and PDA) as potential radiotracers for tumor imaging. The athymic nude mice bearing the MDA-MB-435 human breast cancer xenografts were used to evaluate their biodistribution and metabolic properties. The solution stability data showed that [^{99m}Tc(HYNIC-tetramer)(tricine)(L)] (L = ISONIC and PDA) had a significant (14% and 35%, respectively) at 6 h in the absence of excess ISONIC or PDA coligand. Biodistribution data clearly showed that [^{99m}Tc(HYNIC-tetramer)(tricine)(PDA)] has much lower uptake in most organs of interest than [^{99m}Tc(HYNIC-tetramer)(tricine)(ISONIC)] during the 2 h study period. Results from metabolism studies revealed that ~50% of [^{99m}Tc(HYNIC-tetramer)(tricine)(ISONIC)] remained intact in feces samples at 120 min p.i. Only 10% of [^{99m}Tc(HYNIC-tetramer)(tricine)(PDA)] remained intact in feces samples. The extent of metabolism correlates well with the radiotracer solution stability. The results from this and our previous studies clearly demonstrated that coligands (TPPTS, ISONIC and PDA) have a significant impact on tumor uptake, excretion kinetics and metabolism of the ^{99m}Tc-labeled cyclic RGDfK tetramer. Among the three radiotracers evaluated in this tumor-bearing animal model, [^{99m}Tc(HYNIC-tetramer)(tricine)(TPPTS)] remains the best with respect to blood clearance, tumor uptake, target/background ratios.

INTRODUCTION

Angiogenesis depends on vascular endothelial cell migration and invasion, is regulated by cell adhesion receptors [1-4]. Integrins are such a family of proteins that facilitate cellular adhesion to and migration on extracellular matrix proteins found in intercellular spaces and basement membranes, and regulate cellular entry and withdraw from the cell cycle [5-8]. Integrin $\alpha_v\beta_3$ is a receptor for the extracellular matrix proteins with exposed arginine-glycine-aspartic (RGD) tripeptide sequence [6-10]. Integrin $\alpha_v\beta_3$ is normally expressed at low levels on epithelial cells and mature endothelial cells; but it is highly expressed on the activated endothelial cells in neovasculature of tumors, including osteosarcomas, glioblastomas, melanomas, lung carcinomas, and breast cancer [5,11-18]. It has demonstrated that integrin $\alpha_v\beta_3$ is overexpressed on both endothelial and tumor cells in human breast cancer xenografts [19]. It was also reported that the integrin $\alpha_v\beta_3$ expression correlates well with tumor progression and invasiveness of melanoma, glioma, ovarian and breast cancers [8-18]. The highly restricted expression of integrin $\alpha_v\beta_3$ during tumor growth, invasion and metastasis present an interesting molecular target for early detection of rapidly growing and metastatic tumors [19-23]. The nuclear medicine applications of radiolabeled integrin $\alpha_v\beta_3$ antagonists for imaging tumors by single photon emission computed tomography (SPECT) or positron emission tomography (PET) has been reviewed extensively [23-26].

*To whom correspondence should be addressed. School of Health Sciences, Purdue University, 550 Stadium Mall Drive, West Lafayette, IN 47907. Phone: 765-494-0236; Fax 765-496-1377; Email: lius@pharmacy.purdue.edu.

We and others have been using multimeric cyclic RGD peptides to develop the integrin $\alpha_v\beta_3$-targeted radiotracers to image rapidly growing and metastatic tumors in several tumor-bearing animal models [27-39]. The RGD peptides serve as the targeting biomolecules to carry radionuclide (e.g. ^{99m}Tc, ^{111}In and ^{64}Cu) to the integrin $\alpha_v\beta_3$ overexpressed on both tumor cells and endothelial cells of tumor neovasculature. Recently, we reported the ^{111}In- and ^{64}Cu-labeled cyclic RGDfK tetramer as radiotracers for SPECT and PET imaging of integrin $\alpha_v\beta_3$ expression in tumors [33,37]. Results from *in vitro* assays showed that the tetramer had higher integrin $\alpha_v\beta_3$ binding affinity than the dimer. As a result, ^{111}In(DOTA-tetramer) and ^{64}Cu (DOTA-tetramer) (DOTA = 1,4,7,10-tetraazacyclododecane-1,4,7,10-tetraactic acid) both have high tumor uptake with long tumor retention [33,37]. The tetramer, E{E[c (RGDfK)]$_2$}$_2$, is a much better targeting biomolecule than the dimer, E[c(RGDfK)]$_2$, with respect to the tumor uptake and T/B ratios of their radiotracers [28].

Previously, we reported the evaluation of [^{99m}Tc(HYNIC-tetramer)(tricine)(TPPTS)] (TPPTS = trisodium triphenylphosphine-3,3',3"-trisulfonate) as a new radiotracer for tumor imaging [30]. We found that [^{99m}Tc(HYNIC-tetramer)(tricine)(TPPTS)] had a high tumor uptake with long tumor retention (5.60±0.87 %ID/g and 7.30±1.32 %ID/g at 5 and 120 min postinjection (p.i.), respectively). SPECT images displayed significant localization in tumor as early as 60 min p.i. The combination of high tumor uptake and fast renal excretion suggests that [^{99m}Tc (HYNIC-tetramer)(tricine)(TPPTS)] is a promising radiotracer for non-invasive imaging of integrin $\alpha_v\beta_3$-positive tumors. Since our previous studies have shown that the coligand has a significant impact on biological properties of [^{99m}Tc(HYNIC-dimer)(tricine)(L)] (L = TPPTS, ISONIC and PDA) [28], we decided to explore the impact of coligands on solution stability and biological properties of the ^{99m}Tc-labeled cyclic RGDfK tetramer.

As an extension of our continuing interest in the ^{99m}Tc-labeled cyclic RGD peptides as SPECT radiotracers for tumor imaging, we now present the synthesis and evaluation of two new ternary ligand ^{99m}Tc complexes [^{99m}Tc(HYNIC-tetramer)(tricine)(L)] (L = ISONIC and PDA). The athymic nude mice bearing MDA-MB-435 human breast cancer xenografts were used to evaluate their biological properties. Results from these studies will allow us to compare their biodistribution characteristics (tumor uptake, T/B ratios, excretion kinetics and metabolic stability) with those of [^{99m}Tc(HYNIC-tetramer)(tricine)(TPPTS)] [30].

EXPERIMENTAL SECTION

Materials

Isonicotinic acid (ISONIC), 1,5-pyridinedicarboxylic acid (PDA), and tricine were purchased from *Sigma/Aldrich*. Pentapeptide c(RGDfK) was purchased from Peptides International, Inc. (Louisville, Kentucky). HYNIC-E{E[c(RGDfK)]$_2$}$_2$ (HYNIC-tetramer) and [^{99m}Tc(HYNIC-tetramer)(tricine)(TPPTS)] were prepared according to procedures described in our previous report [30]. Na^{99m}TcO$_4$ was obtained from a commercial DuPont Pharma ^{99}Mo/^{99m}Tc generator, N. Billerica, MA.

Instruments and Methods

The radio-HPLC method used a LabAlliance HPLC system equipped with a β-ram IN-US detector and Zorbax Rx-C$_{18}$ column (4.6 mm × 250 mm, 300 Å pore size). The flow rate was 1 mL/min. The mobile phase was isocratic with 90% solvent A (25 mM ammonium acetate buffer, pH = 5.0) and 10% solvent B (acetonitrile) at 0 – 2 min, followed by a gradient mobile phase going from 10% solvent B at 2 min to 15% solvent B at 5 min and to 20% solvent B at 20 min. The ITLC method used Gelman Sciences silica-gel paper strips and a 1:1 mixture of acetone and saline as the eluent. Using this method, the radiotracer and Na[^{99m}TcO$_4$] migrate to the solvent front and the [^{99m}Tc]colloid remains at the origin.

[^{99m}Tc(HYNIC-tetramer)(tricine)(ISONIC)]

To a clean vial were added 1.0 mL of solution containing 10 mg of ISONIC, 20 mg of tricine, 40 mg of mannitol, 38.5 mg of disodium succinate hexahydrate, and 12.7 mg of succinic acid, were added 0.2 mL of the HYNIC-tetramer solution (100 μg/mL in water), 0.3 mL of Na [$^{99m}TcO_4$] solution (110 – 220 MBq/mL), and 30 μL $SnCl_2$ solution (1 mg/mL in 1.0 N HCl). The vial was heated at 100 °C for 15 – 20 min in a lead-shielded water bath. After heating, the vial was placed back into the lead pig, and allowed to stand at room temperature for ~10 min. A sample of the resulting solution was analyzed by radio-HPLC and TLC. The percentage of [^{99m}Tc]colloid was minimal (<1%). The RCP was >90%. The HPLC retention time was ~14.5 min.

[^{99m}Tc(HYNIC-tetramer)(tricine)(PDA)]

To a clean vial were added 1.0 mL of solution containing 15 mg of PDA, 20 mg of tricine, 40 mg of mannitol, 38.5 mg of disodium succinate hexahydrate, and 12.7 mg of succinic acid, were added 0.2 mL of the HYNIC-tetramer solution (100 μg/mL in water) 0.3 mL of Na [$^{99m}TcO_4$] solution (110 – 220 MBq/mL), and 25 – 30 μL $SnCl_2$ solution (1 mg/mL in 1.0 N HCl). The vial was sealed and heated at 100 °C for 15 min. After cooling to room temperature, a sample of the resulting solution was analyzed by radio-HPLC and TLC. The RCP was >90%. The HPLC retention time was ~14.0 min.

Doses Preparation

For biodistribution studies, [^{99m}Tc(HYNIC-tetramer)(tricine)(L)] (L = ISONIC and PDA) were prepared, and then were purified by radio-HPLC. Volatiles in the HPLC mobile phase were completely removed under the reduced pressure. Doses were prepared by dissolving the purified radiotracer in saline to give a concentration of ~0.37 MBq/mL. The resulting solution was filtered with a 0.20 μm Millex-LG filter to remove any particles before being injected into animals. Each tumor-bearing mouse was injected with 0.1 mL of the dose.

Solution Stability

For solution stability in kit matrix, samples of the reaction mixture containing the radiotracer were analyzed by HPLC at 0, 2, 4, and 6 h post-labeling. For cysteine challenging experiment, the solution containing the radiotracer was mixed with an equal volume of a cysteine solution (1 mg/mL). Samples were analyzed by radio-HPLC at 0, 2, 4, and 6 h. For solution stability after HPLC purification, the radiotracer was separated from reaction mixture. Volatiles were removed under reduced pressure. The residue was dissolved in saline. Samples of the resulting solution were analyzed by HPLC at 0, 2, 4, and 6 h post-labeling.

Determination of Log P Values

The radiotracer was prepared and purified by HPLC. Volatiles were removed completely under vacuum. The residue was dissolved in a mixture of equal volume (3 mL:3 mL) n-octanol and 25 mM phosphate buffer (pH = 7.4). After stirring vigorously for ~20 min, the mixture was centrifuged at a speed of 8,000 rpm for 5 min. Samples (in triplets) from both n-octanol and aqueous layers were counted in a gamma counter (Perkin Elmer Wizard – 1480). The partition coefficients were calculated. The log P value was measured three different times and reported as an average of three different measurements plus the standard deviation.

Animal Studies

Biodistribution, imaging and metabolism studies were performed using athymic nude mice bearing MDA-MB-435 human breast cancer xenografts in compliance NIH animal experiment guidelines (*Principles of Laboratory Animal Care*, NIH Publication No. 86-23, revised 1985).

The animal protocols were approved by the Purdue University Animal Care and Use Committee (PACUC) for biodistribution and metabolism studies.

Tumor-Bearing Mice

Female athymic nu/nu mice (4 – 5 weeks) were purchased from Harlan (Indianapolis, IN). The mice were implanted with 5×10^6 cells of MDA-MB-435 estrogen receptor-negative human breast cancer cells into the mammary fat pad. Tumor cells were grown at 37 °C in Minimal Essential Medium (Alpha Modification) containing 3.7 g of sodium bicarbonate/L, 10% fetal bovine serum v/v, in a humidified atmosphere of 5% carbon dioxide. Four weeks after implantation, animals with tumors in the range of 0.3 – 0.5 g were used for biodistribution studies.

Biodistribution Studies

Sixteen tumor-bearing mice (20 – 25 g) were anesthetized by IP injection of Ketamine (40 – 100 mg/kg) and Xylazine (2 – 5 mg/kg). Once the animal was in surgical plane of anesthesia, the radiotracer (~37 Bq) in saline was administered via tail vein. Four tumor-bearing mice were sacrificed by sodium pentobarbital overdose (150 – 200 mg/kg, IP) at 5, 30, 60 and 120 min p.i. Blood was withdrawn from heart through a syringe. Organs of interest (tumor, brain, eyes, heart, intestine, kidneys, liver, lungs, muscle and spleen) were excised, weighed, and counted on a gamma-counter (Perkin Elmer Wizard – 1480). The organ uptake was calculated as a percentage of the injected dose per gram of wet tissue (%ID/g).

Metabolism

Each tumor-bearing mouse was administered with the radiotracer at a dose of ~3.7 MBq/mice. Urine samples were collected at 2 h p.i. by manual void, and were mixed with equal volume of acetonitrile. The mixture was centrifuged at 8,000 rpm. The supernatant was collected and filtered through a 0.20 micron Millex-LG syringe driven filter unit. The filtrate was analyzed by radio-HPLC. Feces samples were collected at ~120 min p.i. The sample was suspended in a mixture of 50% acetonitrile aqueous solution, and the mixture was vertexed for 5 – 10 min. After centrifuging at 8,000 rpm for 5 min, the supernatant was collected and passed through a 0.20 micron Millex-LG syringe driven filter unit. The filtrate was analyzed by radio-HPLC. Two tumor-bearing mice were used for the metabolism study of each radiotracer.

Imaging Studies

Planar imaging studies on [^{99m}Tc(HYNIC-tetramer)(tricine)(ISONIC)] were performed using the athymic nude mice bearing MDA-MB-435 human breast cancer xenografts. Two tumor-bearing mice (20 – 25 g) were anesthetized by IP injection of Ketamine (40 – 100 mg/kg) and Xylazine (2 – 5 mg/kg). Once the animal was in surgical plane of anesthesia, the radiotracer (~3.7 MBq) in saline was administered via tail vein. Animals were monitored on the gamma camera (PhoGama large field-of-view Anger camera and NucLearMac computer system). Sequential anterior images were collected for 5 min at the specified time (5, 15, 30, 45, 60, 90 and 120 min) using the 256 × 256 image matrix while animals remained under anesthesia. Upon completion of the experiment, the tumor-bearing mice were sacrificed by sodium pentobarbital overdose (150 – 200 mg/kg).

Data and Statistical Analysis

The biodistribution data and T/B ratios are reported as an average plus the standard variation based on the results from four animals for each time point. Comparison between two different radiotracers was also made using the one-way ANOVA test. The level of significance was set at $p < 0.05$.

RESULTS

Radiochemistry

Ternary ligand ^{99m}Tc complexes [^{99m}Tc(HYNIC-tetramer)(tricine)(L)] (L = ISONIC and PDA) were prepared using tricine/ISONIC and tricine/PDA as coligands. Since stannous chloride was used as the reducing agent for the radiolabeling, a large excess of tricine (≥ 20 mg/vial) is needed to prevent formation of [^{99m}Tc]colloid. The radiochemical purity of [^{99m}Tc(HYNIC-tetramer)(tricine)(L)] (L = ISONIC and PDA) was >90% with minimal amount (<0.5%) of [^{99m}Tc]colloid. Their log P values in a mixture of n-octanol and 25 mM phosphate buffer (pH = 7.4) were -3.17±0.12 and -3.10±0.15, respectively. Figure 2 shows the HPLC chromatograms of [^{99m}Tc(HYNIC-tetramer)(tricine)(L)] (L = ISONIC and PDA), and the comparison of their solution stability data with that of [^{99m}Tc(HYNIC-tetramer)(tricine)(TPPTS)] after purification. The HPLC retention times of [^{99m}Tc(HYNIC-tetramer)(tricine)(L)] (L = ISONIC and PDA) were almost identical (14.0 – 14.5 min). Both remained stable in the kit matrix for >12 h. They had a significant decomposition (14% and 35%, respectively) at 6 h after HPLC-purification while [^{99m}Tc(HYNIC-tetramer)(tricine)(TPPTS)] remains stable for >6 h after purification. Apparently, coligands have a significant impact on solution stability of the ^{99m}Tc-labeled cyclic RGDfK tetramer.

The solution structure of [^{99m}Tc(HYNIC-tetramer)(tricine)(L)] (L = ISONIC and PDA) at the tracer level remains unknown. For the last decade, we have been using ternary ligand systems (HYNIC, tricine, water soluble phosphine or pyridine analog) for ^{99m}Tc-labeling of small biomolecules, including chemotactic peptides [40] and LTB_4 antagonists [41,42] for imaging infection/inflammation, integrin $\alpha_v\beta_3$ antagonists for tumor imaging [27-30], and a GPIIb/IIIa antagonist for imaging thrombosis [43-46]. Regardless of the biomolecule, the Tc:HYNIC:L:tricine ratio in [^{99m}Tc(HYNIC-biomolecule)(tricine)(L)] always remains 1:1:1:1 as demonstrated via mixed ligand experiments at the tracer level [43,44], and has been further confirmed by the LC-MS data of [^{99m}Tc(HYNIC-biomolecule)(tricine)(L)] (L = TPPTS and ISONIC) at both macroscopic and tracer levels [47,48]. Based these results, it is reasonable to believe that ternary ligand complexes [^{99m}Tc(HYNIC-tetramer)(tricine)(L)] (L = ISONIC and PDA) contain one HYNIC-tetramer, one tricine, and one monodentate ISONIC or PDA. This conclusion is also supported by the coligand effect observed in this and our previous studies [28]. The HYNIC technology and its utility in the development of target-specific radiopharmaceuticals have been reviewed extensively [49-52].

Biodistribution Characteristics

[^{99m}Tc(HYNIC-tetramer)(tricine)(L)] (L = ISONIC and PDA) were purified by HPLC for biodistribution studies to remove the “unlabeled” HYNIC-tetramer. HPLC purification is needed to study their intrinsic capability to localize in tumor. Biodistribution data for [^{99m}Tc(HYNIC-tetramer)(tricine)(L)] (L = ISONIC, and PDA) are summarized in Tables 1 and 2. The organ uptake is expressed %ID/g. Each data point represents an average of biodistribution data in four tumor-bearing mice.

Figure 3 illustrates the direct comparison of organ uptake and excretion kinetics of [^{99m}Tc(HYNIC-tetramer)(tricine)(L)] (L = TPPTS, ISONIC, and PDA) in tumor, blood, kidneys, liver, lungs and muscle. The biodistribution data for [^{99m}Tc(HYNIC-tetramer)(tricine)(TPPTS)] are obtained in the same tumor-bearing animal model from our previous study [30]. In general, [^{99m}Tc(HYNIC-tetramer)(tricine)(PDA)] had lower uptake in most organs of interest. Both radiotracers had a rapid clearance via renal and hepatobiliary routes. Their blood clearance curves were similar even though [^{99m}Tc(HYNIC-tetramer)(tricine)(ISONIC)] had a higher initial blood activity (7.40±0.41 %ID/g). [^{99m}Tc(HYNIC-tetramer)(tricine)(ISONIC)] had the tumor uptake comparable to that of [^{99m}Tc(HYNIC-tetramer)(tricine)(TPPTS)] at 5 –

60 min p.i. The initial kidney uptake of [^{99m}Tc(HYNIC-tetramer)(tricine)(ISONIC)] (53.81 ±17.33 %ID/g at 5 min p.i.) was much higher than that of [^{99m}Tc(HYNIC-tetramer)(tricine)(TPPTS)] (33.05±5.75 %ID/g) [30], but this difference disappeared between 30 and 120 min p.i. A similar trend was also observed for [^{99m}Tc(HYNIC-tetramer)(tricine)(ISONIC)] in liver and lungs (Figure 3).

Figure 4 shows T/B ratios of [^{99m}Tc(HYNIC-tetramer)(tricine)(L)] (L = TPPTS, ISONIC and PDA). The T/B ratios of [^{99m}Tc(HYNIC-tetramer)(tricine)(TPPTS)] are obtained from our previous study [30]. Even though [^{99m}Tc(HYNIC-tetramer)(tricine)(ISONIC)] had a higher tumor uptake than [^{99m}Tc(HYNIC-tetramer)(tricine)(PDA)], their T/B ratios were well within experimental error, likely due to the high uptake of [^{99m}Tc(HYNIC-tetramer)(tricine)(ISONIC)] in non-tumor organs (Figure 3). Among the three radiotracers evaluated in this specific tumor-bearing animal model, [^{99m}Tc(HYNIC-tetramer)(tricine)(TPPTS)] has the best tumor/liver, tumor/lung and tumor/muscle ratios (Figure 4).

Metabolism

We performed metabolism studies on [^{99m}Tc(HYNIC-tetramer)(tricine)(L)] (L = ISONIC and PDA) using the tumor-bearing mice. Figure 5 shows representative radio-HPLC chromatograms of [^{99m}Tc(HYNIC-tetramer)(tricine)(L)] (L = ISONIC and PDA) in the kit matrix before injection, urine and feces at 120 min p.i. About 35% metabolite(s) from [^{99m}Tc(HYNIC-tetramer)(tricine)(ISONIC)] was detected in the urine sample and more than 50% metabolism was observed in the feces samples at 120 min p.i. (Figure 5). For [^{99m}Tc(HYNIC-tetramer)(tricine)(PDA)], however, about 40% remained intact in urine samples and only ~10% of it remained intact in feces samples at 120 min p.i. Apparently, both radiotracers underwent extensive metabolism, and the extent of metabolism seems to correlate well with their solution stability after HPLC purification.

Planar Imaging

Figure 6 illustrates planar images of the tumor-bearing mouse administered with ~3.7 MBq of [^{99m}Tc(HYNIC-tetramer)(tricine)(ISONIC)] at 30 and 120 min p.i. The breast tumor is clearly visualized as early as 30 min p.i. The activity level in the abdominal region was low at 120 min p.i., which agreed well with the ex vivo biodistribution data at the same time point (Figure 3). However, the image quality is not as good as that in the tumor-bearing mouse administered with [^{99m}Tc(HYNIC-tetramer)(tricine)(TPPTS)] [30].

DISCUSSION

The *in vivo* biodistribution patterns of a radiotracer is determined by several factors, including binding affinity of the targeting biomolecule (cyclic RGDfK tetramer versus dimer), metal chelate and coligands, molecular weight and charge, and lipophilicity [26]. In this study, we found that coligands have a significant impact on solution stability, biodistribution and metabolic characteristics of the ^{99m}Tc-labeled cyclic RGDfK tetramer. When ISONIC and PDA are used as coligands, their ^{99m}Tc complexes, [^{99m}Tc(HYNIC-tetramer)(tricine)(ISONIC)] and [^{99m}Tc(HYNIC-tetramer)(tricine)(PDA)], show 14% and 35% decomposition, respectively, at 6 h after HPLC purification (Figure 2). When TPPTS is used as the coligand, [^{99m}Tc(HYNIC-tetramer)(tricine)(TPPTS)] remains stable for >6 h. We believe that the coligand effect on solution stability of the ^{99m}Tc-labeled RGDfK tetramer is most likely caused by lower electron-donating capability of pyridine-N in ISONIC and PDA as compared to that of TPPTS.

Coligands also have a significant impact on biodistribution and excretion kinetics of the ^{99m}Tc-labeled cyclic RGDfK tetramer. For example, [^{99m}Tc(HYNIC-tetramer)(tricine)

(PDA)] has much lower uptake than [^{99m}Tc(HYNIC-tetramer)(tricine)(ISONIC)] in most organs of interest while the uptake of [^{99m}Tc(HYNIC-tetramer)(tricine)(ISONIC)] is similar to that of [^{99m}Tc(HYNIC-tetramer)(tricine)(TPPTS)] at 5 – 60 min p.i. Since all three radiotracers share the same cyclic RGDfK tetramer, the difference in their biodistribution characteristics is most likely related to their difference in solution stability.

In our previous study, we found that 85% of [^{99m}Tc(HYNIC-tetramer)(tricine)(TPPTS)] remains intact in the feces sample at 120 min p.i. [30]. In this study, >50% of [^{99m}Tc(HYNIC-tetramer)(tricine)(ISONIC)] exists as its metabolized form in feces samples at 120 min p.i. while only ~10% of [^{99m}Tc(HYNIC-tetramer)(tricine)(PDA)] remains intact in feces samples at 120 min p.i. The solution and metabolic stabilities of [^{99m}Tc(HYNIC-tetramer)(tricine)(ISONIC)] are between those of [^{99m}Tc(HYNIC-tetramer)(tricine)(TPPTS)] and [^{99m}Tc(HYNIC-tetramer)(tricine)(PDA)]. This correlates well with the order of electron-donating capability: TPPTS > ISONIC > PDA. The coligand effect has been reported for the ^{99m}Tc-labeled chemotactic peptides [53,54], glycoprotein IIB/IIIa receptor antagonist [46], somatostatin analogs [55,56], interleukin-8 [57], and cholecystokinin (CCK8) peptides [58].

It is important to note that the coligand effect depends largely on the targeting biomolecule. For the ^{99m}Tc-labeled HYNIC-IL-8 conjugate, the use of TPPTS results in the reduced receptor binding affinity, low abscess uptake, and high liver uptake [57]. Nicotinic acid and ISONIC are the best coligands for ^{99m}Tc-labeled HYNIC-IL-8 and CCK8 peptides [58]. For the ^{99m}Tc-labeled cyclic RGDfK dimer, changing coligand had a minimal effect on their tumor-targeting capability [28]. For the ^{99m}Tc-labeled cyclic RGDfK tetramer, TPPTS has the advantage over ISONIC and PDA due to the high solution stability, high tumor uptake, high tumor/liver and tumor/lung ratios of [^{99m}Tc(HYNIC-tetramer)(tricine)(TPPTS)] [30].

CONCLUSION

In conclusion, we evaluated the impact of coligands on solution stability, biodistribution and metabolic characteristics of the ^{99m}Tc-labeled cyclic RGDfK tetramer using athymic nude mice bearing MDA-MB-435 breast cancer xenografts. On the basis of this and our previous studies, we believe that TPPTS is a better coligand than ISONIC or PDA due to high solution stability and favorable biological characteristics of [^{99m}Tc(HYNIC-tetramer)(tricine)(TPPTS)]. However, the choice of coligand for the ^{99m}Tc-labeling of other HYNIC-conjugated biomolecules should be confirmed according to their biodistribution characteristics.

Acknowledgements

Authors would like to thank Dr. Sulma I. Mohammed, the Director of Purdue Cancer Center Drug Discovery Shared Resource, Purdue University, for her assistance with the tumor-bearing animal model. This work is supported, in part, by research grants: 1R01 CA115883-01A2 (S.L.) from National Cancer Institute (NCI), BCTR0503947 (S.L.) from the Susan G. Komen Breast Cancer Foundation, AHA0555659Z (S.L.) from the Greater Midwest Affiliate of American Heart Association, R21 EB003419-02 (S.L.) from National Institute of Biomedical Imaging and Bioengineering (NIBIB) and R21 HL083961-01 from National Heart, Lung, and Blood Institute (NHLBI).

References

1. Folkman J. Angiogenesis in cancer, vascular, rheumatoid and other disease. Nat Med 1995;1:27–31. [PubMed: 7584949]
2. Folkman J. Role of angiogenesis in tumor growth and metastasis. Semin Oncol 2002;29:15–18. [PubMed: 12516034]
3. Mousa SA. Mechanisms of angiogenesis in vascular disorders: potential therapeutic targets. Drugs of the Future 1998;23:51–60.
4. Mousa SA. Integrins as novel drug discovery targets: potential therapeutic and diagnostic implications. Emerging Therapeutic Targets 2000;4:143–153.

5. Bögler O, Mikkelsen T. Angiogenesis in Glioma: molecular mechanisms and roadblocks to translation. Cancer J 2003;9:205–213. [PubMed: 12952305]
6. Hwang R, Varner J. The role of integrins in tumor angiogenesis. Hematol Oncol Clin North Am 2004;18:991–1006. [PubMed: 15474331]
7. Jin H, Varner J. Integrins: roles in cancer development and as treatment targets. Br J Cancer 2004;90:561–565. [PubMed: 14760364]
8. Kumar CC. Integrin $\alpha_v\beta_3$ as a therapeutic target for blocking tumor-induced angiogenesis. Curr Drug Targets 2003;4:123–131. [PubMed: 12558065]
9. Brooks PC, Clark RAF, Cheresh DA. Requirement of vascular integrin $\alpha_v\beta_3$ for angiogenesis. Science 1994;264:569–571. [PubMed: 7512751]
10. Friedlander M, Brooks PC, Shaffer RW, Kincaid CM, Varner JA, Cheresh DA. Definition of two angiogenic pathways by distinct α_v integrins. Science 1995;270:1500–1502. [PubMed: 7491498]
11. Horton MA. The $\alpha_v\beta_3$ integrin "vitronectin receptor". Int J Biochem Cell Biol 1997;29:721–725. [PubMed: 9251239]
12. Bello L, Francolini M, Marthyn P, Zhang JP, Carroll RS, Nikas DC, Strasser JF, Villani R, Cheresh DA, Black PM. $\alpha_v\beta_3$ and $\alpha_v\beta_3$ Integrin expression in glioma periphery. Neurosurgery 2001;49:380–389. [PubMed: 11504114]
13. Meitar D, Crawford SE, Rademaker AW, Cohn SL. Tumor angiogenesis correlates with metastatic disease, N-*myc*-amplification, and poor outcome in human neuroblastoma. J Clinical Oncol 1996;14:405–414. [PubMed: 8636750]
14. Gasparini G, Brooks PC, Biganzoli E, Vermeulen PB, Bonoldi E, Dirix LY, Ranieri G, Miceli R, Cheresh DA. Vascular integrin $\alpha_v\beta_3$: a new prognostic indicator in breast cancer. Clinical Cacer Res 1998;4:2625–2634.
15. Albelda SM, Mette SA, Elder DE, Stewart RM, Damjanovich L, Herlyn M, Buck CA. Integrin distribution in maliganant melanoma: association of the β_3 subunit with tumor progression. Cancer Res 1990;50:6757–6764. [PubMed: 2208139]
16. Falcioni R, Cimino L, Gentileschi MP, D'Agnano I, Zupi G, Kennel SJ, Sacchi A. Expression of β_1, β_3, β_4, and β_5 integrins by human lung carcinoma cells of different histotypes. Exp Cell Res 1994;210:113–122. [PubMed: 7505746]
17. Sengupta S, Chattopadhyay N, Mitra A, Ray S, Dasgupta S, Chatterjee A. Role of $\alpha_v\beta_3$ integrin receptors in breast tumor. J Exp Clin Cancer Res 2001;20:585–590. [PubMed: 11876555]
18. Felding-Habermann B, Mueller BM, Romerdahl CA, Cheresh DA. Involvement of integrin alpha V gene expression in human melanoma tumorigenicity. J Clin Invest 1992;89:2018–2022. [PubMed: 1376331]
19. Zitzmann S, Ehemann V, Schwab M. Arginine-Glycine-Aspartic acid (RGD)-peptide binds to both tumor and tumor endothelial cells in vivo. Cancer Res 2002;62:5139–5143. [PubMed: 12234975]
20. Weber WA, Haubner R, Vabuliene E, Kuhnast B, Wester HJ, Schwaiger M. Tumor angiogenesis targeting using imaging agents. Q J Nucl Med 2001;45:179–182. [PubMed: 11476168]
21. Costouros NG, Diehn FE, Libutti SK. Molecular imaging of tumor angiogenesis. J Cell Biochem Suppl 2002;39:72–78. [PubMed: 12552605]
22. van de Wiele C, Oltenfreiter R, De Winter O, Signore A, Slegers G, Dierckx RA. Tumor angiogenesis pathways: related clinical issues and implications for nuclear medicine imaging. Eur J Nucl Med 2002;29:699–709.
23. Liu S, Robinson SP, Edwards DS. Integrin $\alpha_v\beta_3$ directed radiopharmaceuticals for tumor imaging. Drugs of the Future 2003;28:551–564.
24. Haubner R, Wester HR. Radiolabeled tracers for imaging of tumor angiogenesis and evaluation of anti-angiogenic therapies. Curr Pharm Des 2004;10:1439–1455. [PubMed: 15134568]
25. Chen XY. Multimodality imaging of tumor integrin $\alpha_v\beta_3$ expression. Mini-Reviews in Medicinal Chemistry 2006;6:227–234. [PubMed: 16472190]
26. Liu S. Radiolabeled multimeric cyclic RGD peptides as integrin $\alpha_v\beta_3$-targeted radiotracers for tumor imaging. Molecular Pharmaceuticals 2006;3:472–487.

27. Liu S, Edwards DS, Ziegler MC, Harris AR, Hemingway SJ, Barrett JA. ^{99m}Tc-Labeling of a hydrazinonicotinamide-conjugated vitronectin receptor antagonist useful for imaging tumors. Bioconj Chem 2001;12:624–629.
28. Liu S, Hsieh WY, Kim YS, Mohammed SI. Effect of coligands on biodistribution characteristics of ternary ligand ^{99m}Tc complexes of a HYNIC-conjugated cyclic RGDfK dimer. Bioconj Chem 2005;16:1580–1588.
29. Jia B, Shi J, Yang Z, Xu B, Liu Z, Zhao H, Liu S, Wang F. ^{99m}Tc-labeled cyclic RGDfK dimer: initial evaluation for SPECT imaging of glioma integrin $\alpha_v\beta_3$ expression. Bioconj Chem 2006;17:1069–1076.
30. Liu S, Hsieh WY, Jiang Y, Kim YS, Sreerama SG, Chen XY, Jia B, Wang F. Evaluation of a ^{99m}Tc-labeled cyclic RGD tetramer for non-invasive imaging integrin $\alpha_v\beta_3$-positive breast cancer. Bioconj Chem 2007;18:438–446.
31. Chen XY, Liu S, Hou YP, Tohme M, Park R, Bading JR, Conti PS. MicroPET imaging of breast cancer $\alpha_v\beta_3$-integrin expression with ^{64}Cu-labeled dimeric RGD peptides. Mol Imag Biol 2004;6:350–359.
32. Chen XY, Tohme M, Park R, Hou Y, Bading JR, Conti PS. MicroPET imaging of breast cancer α_v-integrin expression with ^{18}F-labeled dimeric RGD peptide. Mol Imaging 2004;3:96–104. [PubMed: 15296674]
33. Wu Y, Zhang XZ, Xiong ZM, Cheng Z, Fisher DR, Liu S, Gambhir SS, Chen X-Y. MicroPET imaging of glioma α_v-integrin expression using ^{64}Cu-labeled tetrameric RGD peptide. J Nucl Med 2005;46:1707–1718. [PubMed: 16204722]
34. Janssen ML, Oyen WJG, Dijkgraaf I, Massuger LF, Frielink C, Edwards DS, Rajopadhye M, Boonstra H, Corstens FH, Boerman OC. Tumor targeting with radiolabeled $\alpha_v\beta_3$ integrin binding peptides in a nude mouse model. Cancer Res 2002;62:6146–6151. [PubMed: 12414640]
35. Janssen M, Oyen WJG, Massuger LFAG, Frielink C, Dijkgraaf I, Edwards DS, Rajopadyhe M, Corstens FHM, Boerman OC. Comparison of a monomeric and dimeric radiolabeled RGD-peptide for tumor targeting. Cancer Biotherapy & Radiopharm 2002;17:641–646.
36. Dijkgraaf I, Liu S, Kruijtzer JAW, Soede AC, Oyen WJG, Liskamp RMJ, Corstens FHM, Boerman OC. Effect of linker variation on the in vitro and in vivo characteristics of an ^{111}In-labeled RGD Peptide. Nucl Med Biol 2007;34:29–35. [PubMed: 17210459]
37. Dijkgraaf I, John AW, Kruijtzer JAW, Liu S, Soede A, Oyen WJG, Corstens FHM, Liskamp RMJ, Boerman OC. Improved targeting of $\alpha_v\beta_3$ integrin by multimerization of RGD peptides. Eur J Nucl Med Mol Imaging 2007;34:267–273. [PubMed: 16909226]
38. Poethko T, Schottelius M, Thumshirn G, Herz M, Haubner R, Henriksen G, Kessler H, Schwaiger M, Wester HJ. Chemoselective pre-conjugate radiohalogenation of unprotected mono- and multimeric peptides via oxime formation. Radiochimica Acta 2004;92:317–327.
39. Thumshirn G, Hersel U, Goodman SL, Kessler H. Multimeric cyclic RGD peptides as potential tools for tumor targeting: solid-phase peptide synthesis and chemoselective oxime ligation. Chem Eur J 2003;9:2717–2725.
40. Edwards DS, Liu S, Ziegler MC, Harris AR, Crocker AC, Heminway SJ, Barrett JA, Bridger GJ, Abrams MJ, Higgins JD III. RP463: A stabilized technetium-99m complex of a hydrazino nicotinamide conjugated chemotactic peptide for infection imaging. Bioconj Chem 1999;10:884–891.
41. Liu S, Edwards DS, Ziegler MC, Harris AR. ^{99m}Tc-labeling of a hydrazinonictotinamide-conjugated LTB4 receptor antagonist useful for imaging infection. Bioconj Chem 2002;13:881–886.
42. van Eerd JEM, Oyen WJG, Harris TD, Rennen HJJM, Edwards DS, Liu S, Ellars CE, Corstens FHM, Boerman OC. A bivalent leukotriene B4 antagonist for scintigraphic imaging of infectious foci. J Nucl Med 2003;44:1087–1091. [PubMed: 12843226]
43. Edwards DS, Liu S, Barrett JA, Harris AR, Looby RJ, Ziegler MC, Heminway SJ, Carroll TR. A new and versatile ternary ligand system for technetium radiopharmaceuticals: water soluble phosphines and tricine as coligands in labeling a hydrazino nicotinamide-modified cyclic glycoprotein IIb/IIIa receptor antagonist with ^{99m}Tc. Bioconj Chem 1997;8:146–154.

44. Liu S, Edwards DS, Harris AR. A novel ternary ligand system for technetium radiopharmaceuticals: imine-N containing heterocycles as coligands in labeling a hydrazinonicotinamide-modified cyclic platelet glycoprotein IIb/IIIa receptor antagonist with ^{99m}Tc. Bioconj Chem 1998;9:583–595.
45. Edwards DS, Liu S, Harris AR, Ewels BA. ^{99m}Tc-labeling hydrazones of a hydrazinonicotinamide conjugated cyclic peptide. Bioconj Chem 1999;10:803–807.
46. Barrett JA, Crocker AC, Damphousse DJ, Heminway SJ, Liu S, Edwards DS, Lazewatsky JL, Kagan M, Mazaika TJ, Carroll TR. Biological evaluation of thrombus imaging agents utilizing water soluble phosphines and tricine as coligands when used to label a hydrazinonicotinamide-modified cyclic glycoprotein IIb/IIIa receptor antagonist with ^{99m}Tc. Bioconj Chem 1997;8:155–160.
47. Liu S, Ziegler MC, Edwards DS. Radio-LC-MS for the characterization of ^{99m}Tc-labeled bioconjugates. Bioconj Chem 2000;11:113–117.
48. Liu S, Edwards DS, Harris AR, Heminway SJ, Barrett JA. Technetium complexes of a hydrazinonicotinamide-conjugated cyclic peptide and 2-hydrazinopyridine: Synthesis and characterization. Inorg Chem 1999;38:1326–1335. [PubMed: 11670921]
49. Liu S, Edwards DS, Barrett JA. ^{99m}Tc-labeling of highly potent small peptides. Bioconj Chem 1997;8:621–636.
50. Liu S. 6-Hydrazinonicotinamide derivatives as bifunctional coupling agents for ^{99m}Tc-labeling of small biomolecules. Topics in Current Chem 2005;252:117–153.
51. Liu S, Edwards DS. ^{99m}Tc-labeled small peptides as diagnostic radiopharmaceuticals. Chem Rev 1999;99:2235–2268. [PubMed: 11749481]
52. Liu S, Edwards DS. New Radiopharmaceuticals for imaging infection and inflammation. Drugs of the Future 2001;26:375–382.
53. Babich JW, Fischman AJ. Effect of “co-ligand” on the biodistribution of ^{99m}Tc-labeled hydrazino nicotinic acid derivatized chemotactic peptides. Nucl Med Biol 1995;22:25–30. [PubMed: 7735166]
54. Babich JW, Coco WG, Barrow SA, Fischman AJ, Femia FJ, Zubieta J. ^{99m}Tc-labeled chemotactic peptides: influence of coligand on distribution of molecular species and infection imaging properties. Synthesis and structural characterization of model complexes with the {Re(η^2-HNNC$_5$H$_4$N)(η^1-NNC$_5$H$_4$N)} core. Inorg Chim Acta 2000;309:123–136.
55. Decristoforo C, Mather SJ. Technetium-99m somatostatin analogues: effect of labeling methods and peptide sequence. Eur J Nucl Med 1999;26:869–876. [PubMed: 10436200]
56. Decristoforo C, Mather SJ. ^{99m}Tc-labeled peptide-HYNIC conjugates: effect of lipophilicity and stability on biodistribution. Nucl Med Biol 1999;26:389–396. [PubMed: 10382842]
57. Rennen HJJM, van Eerd JE, Oyen WJG, Corstens FHM, Edwards DS, Boerman OC. Effects of coligand variation on the in vivo characteristics of Tc-99m-labeled interleukin-8 in detection of infection. Bioconj Chem 2002;13:370–377.
58. Laverman P, Béhé M, Oyen WJG, Willems PHGM, Corstens FHM, Behr TM, Boerman OC. Two technetium-99m-labeled cholecystokinin-8 (CCK8) peptides for scintigraphic imaging of CCK receptors. Bioconj Chem 2004;15:561–568.

ABBREVIATIONS

HYNIC-tetramer
: [2-[[[5-[carbonyl]-2-pyridinyl]hydrazono]methyl]benzenesulfonic acid]-Glu{Glu[cyclo(Lys-Arg-Gly-Asp-D-Phe)]-cyclo(Lys-Arg-Gly-Asp-D-Phe)}-{Glu[cyclo(Lys-Arg-Gly-Asp-D-Phe)]-cyclo(Lys-Arg-Gly-Asp-D-Phe)}

TPPTS
: trisodium triphenylphosphine-3,3’,3”-trisulfonate

ISONIC
: isonicotinic acid

PDA
: 2,5-pyridinedicarboxylic acid

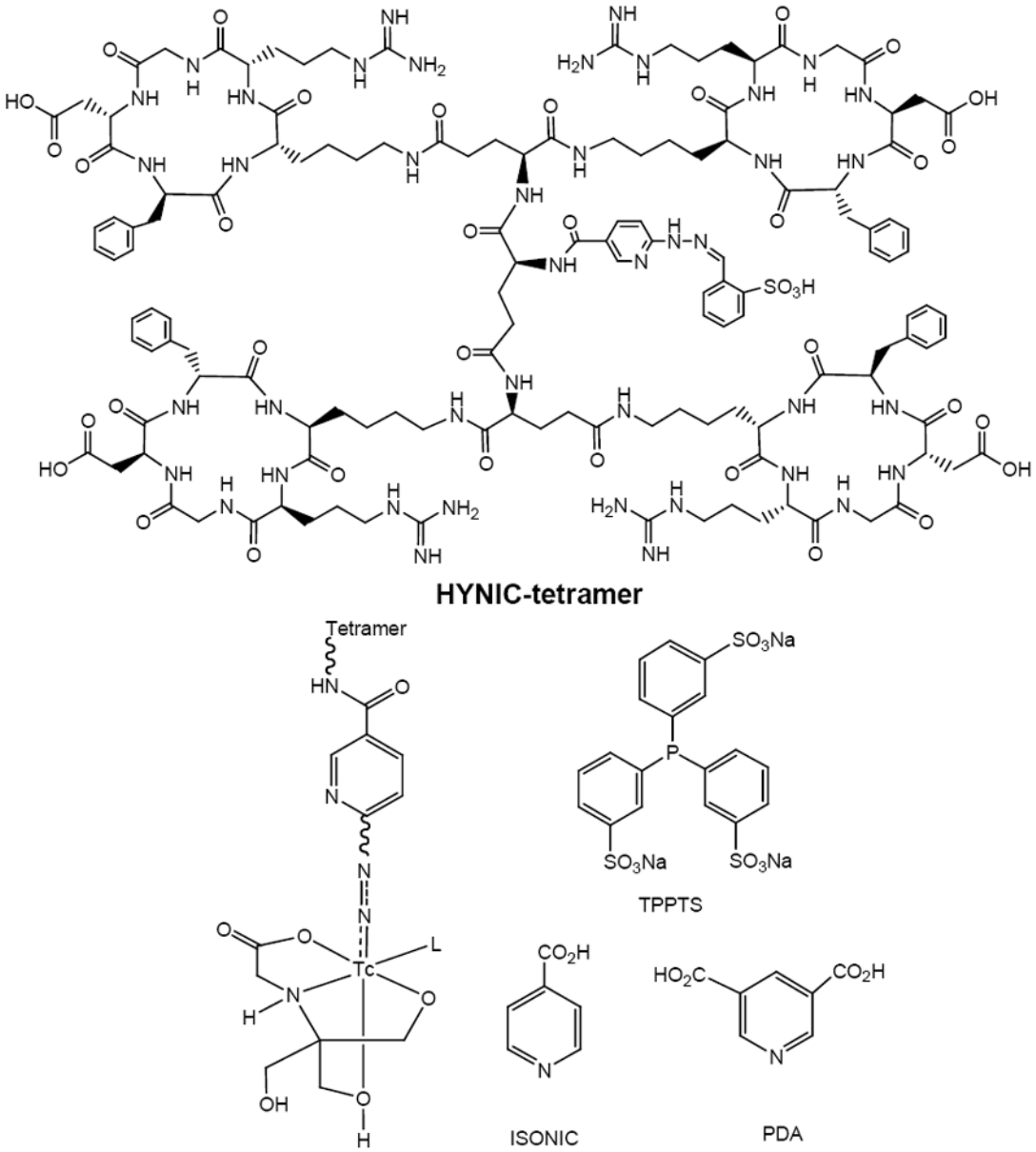

Figure 1.
Structures of HYNIC-tetramer and its ternary ligand complexes [^{99m}Tc(HYNIC-tetramer)(tricine)(L)] (L = TPPTS, ISONIC and PDA).

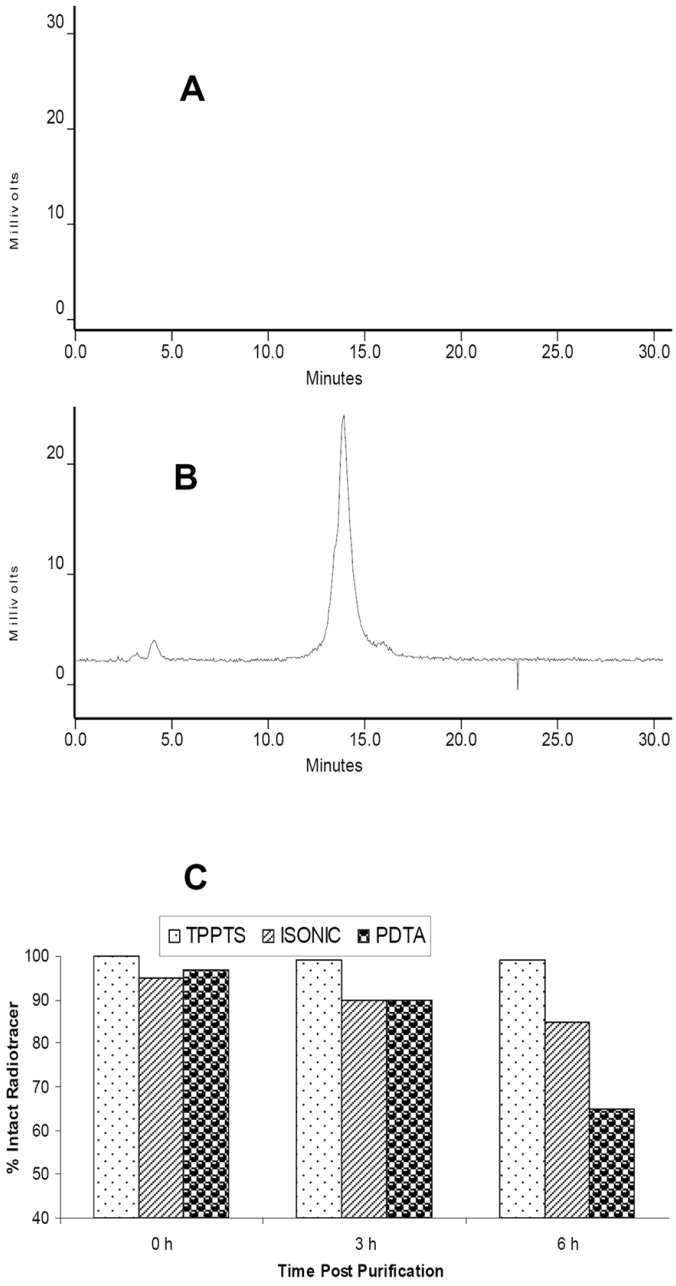

Figure 2.
Typical radio-HPLC chromatograms of [^{99m}Tc(HYNIC-tetramer)(tricine)(ISONIC)] (A) and [^{99m}Tc(HYNIC-tetramer)(tricine)(PDA)] (B) in the kit matrix, and their solution stability data after HPLC purification (C). The solution stability data for [^{99m}Tc(HYNIC-tetramer)(tricine)(TPPTS)] were obtained from our previous study [30].

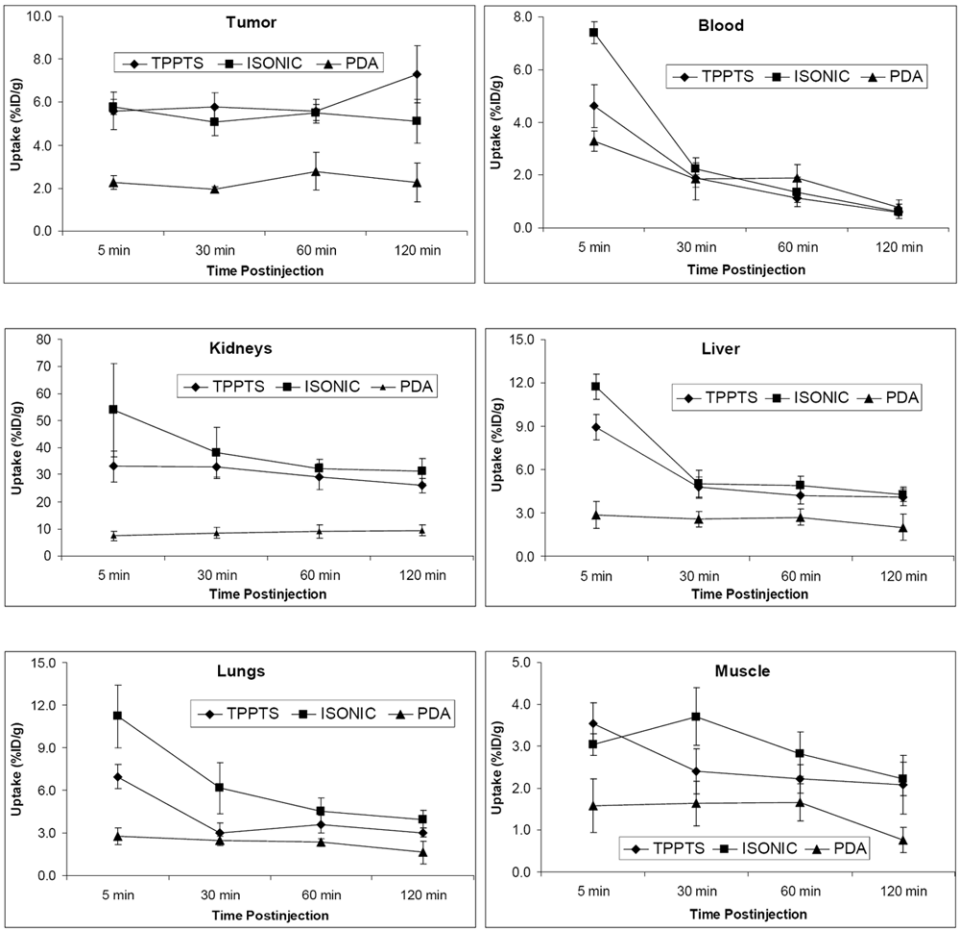

Figure 3.

Coligand effect on tumor uptake and excretion kinetics of ternary ligand complexes [^{99m}Tc (HYNIC-tetramer)(tricine)(L)] (L = TPPTS, ISONIC, and PDA) in blood, kidneys, liver, lungs, and muscle with respect to their in athymic nude mice bearing MDA-MB-435 human breast cancer xenografts. Biodistribution data for [^{99m}Tc(HYNIC-tetramer)(tricine)(TPPTS)] are obtained from our previous studies in the same tumor-bearing animal model [30].

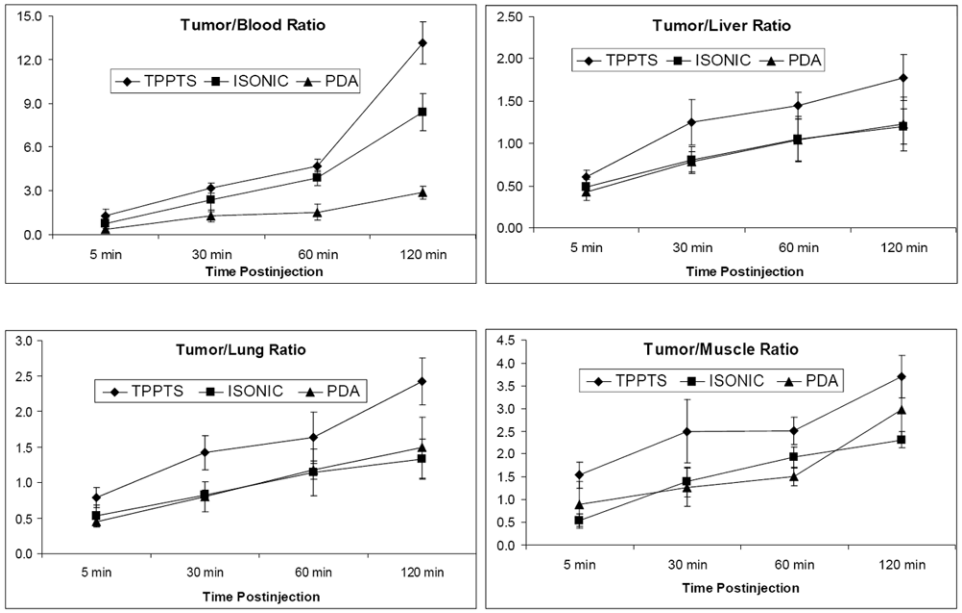

Figure 4.

Coligand effect on T/B ratios of [^{99m}Tc(HYNIC-tetramer)(tricine)(L)] (L = TPPTS, ISONIC, and PDA) in athymic nude mice bearing MDA-MB-435 human breast cancer xenografts. T/B ratios for [^{99m}Tc(HYNIC-tetramer)(tricine)(TPPTS)] are obtained from previous studies in the same tumor-bearing animal model [30].

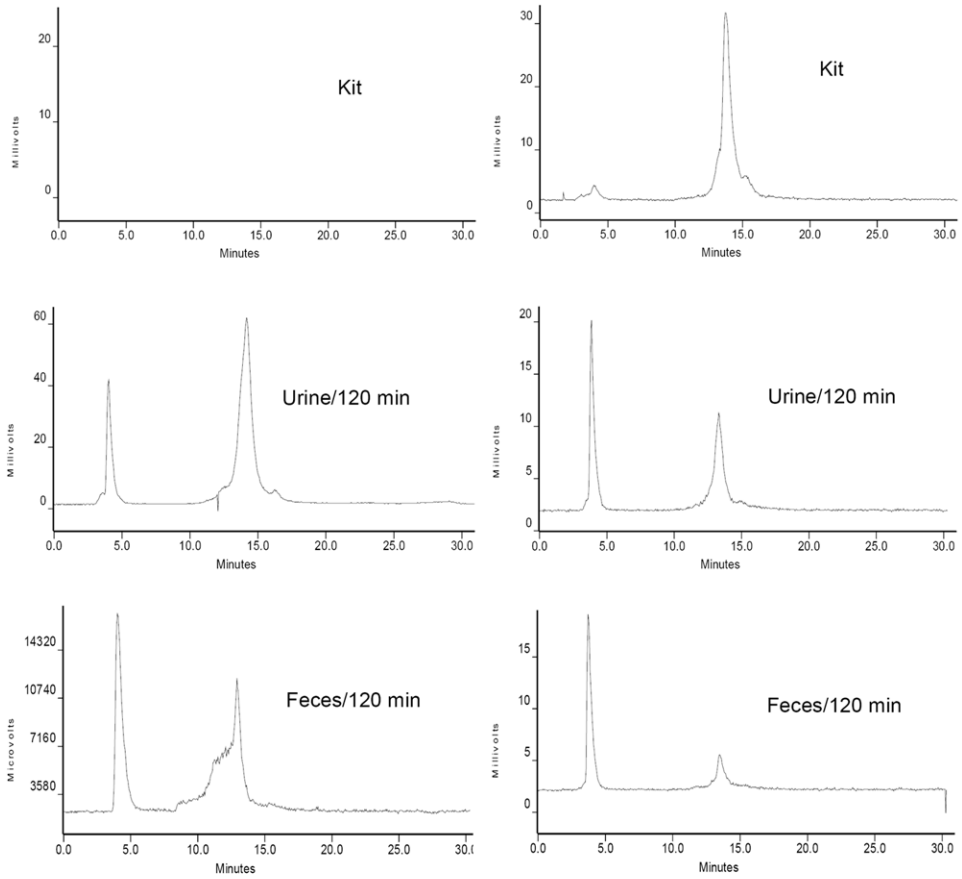

Figure 5.

Radio-HPLC chromatograms of [^{99m}Tc(HYNIC-dimer)(tricine)(ISONIC)] (left) and [^{99m}Tc(HYNIC-tetramer)(tricine)(PDA)] (right) in the kit matrix before injection, in the urine and feces at 120 min postinjection. Each tumor-bearing mouse was administered with ~ 3.7 MBq of radiotracer. Two tumor-bearing mice were used for each radiotracer.

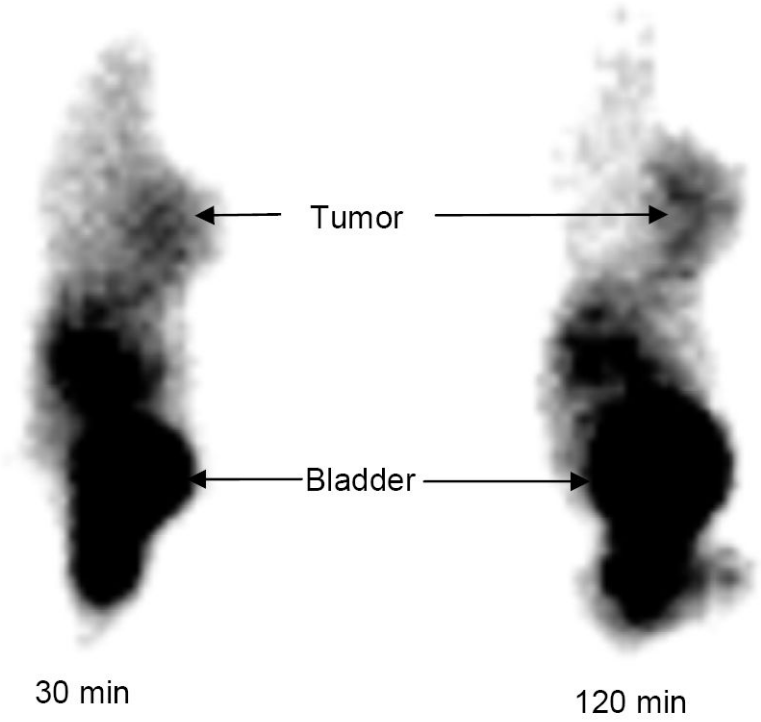

Figure 6.
Representative static planar images of the tumor-bearing nude mice administered with ~3.7 MBq of [^{99m}Tc(HYNIC-dimer)(tricine)(ISONIC)] at 15 and 120 min p.i. Arrows indicate presence of tumor and bladder.

Table 1

Biodistribution data of [^{99m}Tc(HYNIC-tetramer)(tricine)(ISONIC)] in athymic nude mice bearing MDA-MB-435 human breast cancer xenografts. The organ uptake is expressed %ID/g. Each data point represents an average of biodistribution data in four animals

Organ	5 min	30 min	60 min	120 min
Blood	7.40±0.41	2.23±0.23	1.35±0.55	0.61±0.27
Brain	4.44±8.03	0.75±0.41	0.47±0.06	0.33±0.03
Eyes	14.52±4.45	6.51±3.51	3.58±0.73	2.82±0.29
Heart	8.02±0.91	3.06±0.69	2.66±0.81	2.33±0.41
Intestine	16.58±6.07	7.98±2.62	8.09±3.27	7.58±2.33
Kidneys	53.81±17.33	38.28±9.08	32.20±3.46	31.23±4.60
Liver	11.73±0.87	5.03±0.93	4.93±0.63	4.28±0.51
Lungs	11.23±2.21	6.15±1.79	4.53±0.93	3.97±0.64
Muscle	3.50±0.26	3.71±0.69	2.82±0.53	2.22±0.39
Tumor	5.77±0.35	5.07±0.63	5.51±0.37	5.12±1.02
Tumor/Blood	0.78±0.37	2.36±0.32	3.87±0.51	8.40±1.26
Tumor/Liver	0.49±0.09	0.86±0.16	1.05±0.27	1.20±0.21
Tumor/Lung	0.53±0.07	0.82±0.21	1.14±0.13	1.33±0.43
Tumor/Muscle	0.53±0.46	1.39±0.33	1.93±0.23	2.31±0.18

Table 2

Biodistribution data of [^{99m}Tc(HYNIC-tetramer)(tricine)(PDA)] in athymic nude mice bearing MDA-MB-435 human breast cancer xenografts. The organ uptake is expressed %ID/g. Each data point represents an average of biodistribution data in four animals

Organ	5 min	30 min	60 min	120 min
Blood	3.28 ± 0.37	1.85 ± 0.79	1.89 ± 0.51	0.78 ± 0.28
Brain	0.16 ± 0.04	0.15 ± 0.03	0.14 ± 0.04	0.12 ± 0.05
Eyes	1.12 ± 0.41	1.16 ± 0.36	0.85 ± 0.07	0.94 ± 0.19
Heart	1.95 ± 0.57	1.53 ± 0.10	1.23 ± 0.21	0.99 ± 0.40
Intestine	2.57 ± 2.22	2.93 ± 0.21	3.41 ± 0.72	2.77 ± 1.28
Kidney	7.39 ± 1.75	8.52 ± 1.94	8.88 ± 2.44	9.43 ± 1.90
Liver	2.86 ± 0.95	2.55 ± 0.52	2.69 ± 0.55	1.99 ± 0.90
Lungs	2.78 ± 0.60	2.45 ± 0.33	2.34 ± 0.26	1.62 ± 0.78
Muscle	1.58 ± 0.64	1.64 ± 0.53	1.67 ± 0.44	0.77 ± 0.30
Spleen	1.39 ± 0.55	1.40 ± 0.23	1.43 ± 0.32	1.35 ± 0.58
Tumor	2.20 ± 0.32	1.94 ± 0.12	2.79 ± 0.88	2.27 ± 0.89
Tumor/Blood	0.37 ± 0.13	1.26 ± 0.72	1.52 ± 0.54	2.88 ± 0.45
Tumor/Liver	0.43 ± 0.10	0.78 ± 0.12	1.04 ± 0.25	1.23 ± 0.32
Tumor/Lung	0.45 ± 0.15	0.80 ± 0.07	1.18 ± 0.33	1.49 ± 0.28
Tumor/Muscle	0.90 ± 0.49	1.27 ± 0.42	1.51 ± 0.20	2.97 ± 0.69